Four-Gyre Circulation in a Barotropic Model with Double-Gyre Wind Forcing

RICHARD J. GREATBATCH

Department of Oceanography, Dalhousie University, Halifax, Nova Scotia, Canada

B. T. NADIGA

Earth and Environmental Sciences, Los Alamos National Laboratory, Los Alamos, New Mexico

8 July 1998 and 20 September 1999

ABSTRACT

Results from a barotropic vorticity equation model driven by symmetric, double-gyre wind forcing are described. The authors work in a regime in which the model reaches a state of turbulent equilibrium. The time-average of the statistically steady state exhibits a four-gyre structure, in contrast to the usual two gyres associated with symmetric double-gyre wind forcing. The four-gyre structure is found in model runs using either free-slip or superslip boundary conditions, and with either Laplacian or biharmonic mixing for the dissipation. It is shown that the vorticity budget of both the inner and outer gyres is dominated by a balance between the wind stress curl and the divergence of the eddy potential vorticity flux, with the explicit dissipation playing a much smaller role. The two inner gyres circulate in the same sense as the wind stress curl and are equilibriated, for the most part, by the eddy flux of potential vorticity. The outer gyres, on the other hand, circulate in the opposite sense to the wind stress curl and are driven by the eddy flux of potential vorticity. It is shown that the gross features of the time-averaged state can be reproduced by a parameterized model in which the divergent part of the potential vorticity flux is represented as a downgradient transfer, and a boundary condition of no normal flux of potential vorticity is applied along the model boundaries. In contrast to the eddy resolving model, the four-gyre structure in the parameterized model depends strongly on the choice of side boundary condition.

1. Introduction

A feature of unforced geostrophic turbulence with weak dissipation is the tendency for potential vorticity to homogenize (e.g., Bretherton and Haidvogel 1976; Cummins 1992; Wang and Vallis 1994; Dukowicz and Greatbatch 1999; by ''weak'' dissipation, we mean dissipation that is strong enough to influence the dynamics, but not so strong as to suppress turbulence). Associated with the homogenization, the circulation splits into two separated gyres, one at the northern end of the basin and the other at the southern end. The tendency toward homogenization is consistent with parameterizing the divergent part of the eddy potential vorticity flux as a flux down the mean potential vorticity gradient (Rhines and Young 1982). Potential vorticity homogenization is also a feature of wind-driven, multilevel quasigeostrophic models (e.g., Holland et al. 1984) and model simulations of free jets (e.g., Jayne et al. 1996).

Recently there has been much interest in the response of simple models driven by double-gyre wind forcing. For example, it is has been shown that such models can exhibit multiple equilibria and low frequency variability (Cessi and Ierley 1995; Jiang et al. 1995; McCalpin 1995; McCalpin and Haidvogel 1996; Nadiga and Holm 1997). In this paper, we consider the barotropic vorticity equation under double-gyre wind forcing in a highly turbulent regime that has weak dissipation. We find time-mean circulations that are characterized by a four gyre structure. The two inner gyres circulate in the same sense as the wind stress curl forcing and are equilibriated by the eddy flux of potential vorticity, while the two outer gyres correspond to the northern and southern gyres found in geostrophic turbulence experiments and are driven by the eddy flux of potential vorticity. We show that the result is robust in the sense that it is obtained in experiments that use either Laplacian or biharmonic mixing of momentum, either free or superslip boundary conditions, and for two widely different Rossby numbers. We also show that the four-gyre structure is reproduced in a model in which the divergent part of the eddy flux of potential vorticity is parameterized as a downgradient transfer and a condition of no normal flux of potential vorticity is applied along the model boundaries.

Griffa and Salmon (1989) have suggested that Fo-

Corresponding author address: Dr. Richard J. Greatbatch, Department of Oceanography, Dalhousie University, Halifax, NS B3H 4J1, Canada.
E-mail: richard.greatbatch@dal.ca

fonoff-like inertial gyres, to which the outer two of our four gyres correspond, are inhibited in the barotropic vorticity equation under the conventional double-gyre wind forcing we use. Ozgokmen and Chassignet (1998) reiterate the above. These authors show the emergence of Fofonoff-like flows in a two-level quasigeostrophic model under double-gyre wind forcing and attribute their emergence to the presence of density stratification. Our results, on the other hand, demonstrate that a four-gyre structure can indeed emerge under double-gyre wind forcing in a single-layer barotropic model. The reason is that in the highly turbulent regime in which we work, the eddy flux of potential vorticity dominates the explicit dissipation in the vorticity balance and balances the vorticity input from the wind stress forcing. The eddy flux of potential vorticity leads to a tendency for potential vorticity to homogenize and it is this tendency, in the presence of the northern and southern boundaries, that drives the outer gyres.

The plan of the paper is as follows. Section 2 describes the basic model and section 3 the model results. Section 4 describes the parameterized model and section 5 provides a summary and discussion.

2. The basic model

We integrate the barotropic vorticity equation

$$\frac{\partial q}{\partial t} + J(\psi, q) = F - D, \tag{1}$$

where $q = \nabla^2\psi + \beta y$ is the potential vorticity, ψ is the velocity streamfunction, F is the forcing, D is the dissipation and $J(\ ,\ )$ is the Jacobian operator given by

$$J(\psi, q) = -\frac{\partial \psi}{\partial y}\frac{\partial q}{\partial x} + \frac{\partial \psi}{\partial x}\frac{\partial q}{\partial y}. \tag{2}$$

We work in a rectangular, closed basin on a beta plane with the y coordinate increasing northward and the x coordinate eastward. The center of the basin is at $y = 0$, and the northern and southern boundaries are at $y = \pm L$, respectively, with the western and eastern boundaries at $x = 0$ and $x = L$ (see Fig. 1).

A nondimensionalization of (1) using the length scale L, a timescale L/U, and the Sverdrup velocity scale $U = \pi\tau_0/\rho H\beta L$, where τ_0 is the amplitude of the wind stress (in N m^{-2}), ρ the density and H the depth of the fluid, leaves the form of (1) unchanged, but leads to

$$q = \mathrm{Ro}\nabla^2\psi + y, \tag{3}$$

where $\mathrm{Ro} = (\delta_i/L)^2 = U/\beta L^2$ is the Rossby number and $\delta_i = (U/\beta)^{1/2}$ is the Rhines scale.

The wind forcing F has a double-gyre structure given by

$$F = \sin(\pi y). \tag{4}$$

Note that the amplitude of the wind forcing is unity given the (Sverdrup) scaling used in the nondimensionalization of velocity. The dissipation D is due to either Laplacian or biharmonic mixing of momentum. For Laplacian mixing

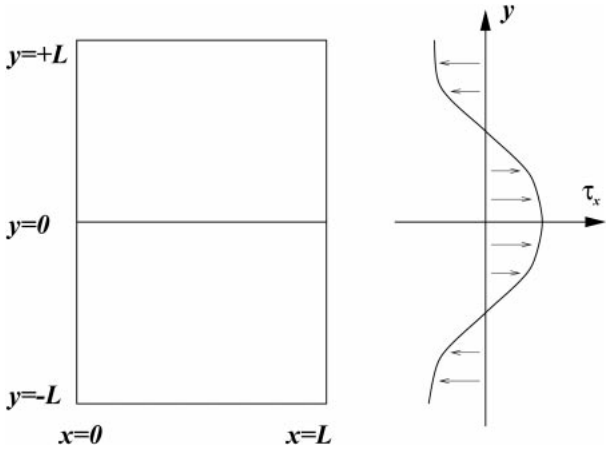

FIG. 1. Schematic of the model.

$$D = -\left(\frac{\delta_2}{L}\right)^3 \nabla^2\zeta, \tag{5}$$

where $\zeta = \nabla^2\psi$ is the relative vorticity and either a free-slip boundary condition of

$$\zeta = 0 \tag{6}$$

or a superslip boundary condition of

$$\frac{\partial \zeta}{\partial n} = 0 \tag{7}$$

is applied along the boundaries. Here, $\partial/\partial n$ denotes a derivative normal to the boundary, and δ_2 is the Munk scale given by $(\delta_2/L)^3 = A_2/\beta L^3$. The use of free-slip and superslip boundary conditions in geostrophic turbulence experiments, and their justification, has been discussed in detail by Cummins (1992) and Wang and Vallis (1994). For biharmonic friction

$$D = \left(\frac{\delta_4}{L}\right)^5 \nabla^4\zeta, \tag{8}$$

with

$$\zeta = 0 \tag{9}$$

and

$$\frac{\partial^2 \zeta}{\partial n^2} = 0 \tag{10}$$

along the boundaries. Here $(\delta_4/L)^5 = A_4/\beta L^5$ and δ_4 is the width of the Munk boundary layer appropriate to biharmonic friction.

Equation (1) is finite differenced using the Arakawa discretization (Arakawa 1966) for the Jacobian and centered differencing for the spatial discretization of the other terms. In order to run the model with the superslip

TABLE 1. The model experiments.

Run	Dissipation	Boundary condition	Munk scale	Rhines scale	Grid spacing
1	Laplacian	Freeslip	0.04	0.10	0.02
2	Laplacian	Superslip	0.04	0.10	0.02
3	Biharmonic	Freeslip	0.04	0.10	0.02
4	Biharmonic	Freeslip	0.02	0.04	0.01
5	Laplacian	Freeslip	0.03	0.04	0.02
6	Parameterized	$\partial q/\partial n = 0$	0.08	0.04	0.04

boundary condition (7), it is necessary to update q on the boundary of the model domain. We do this using the method discussed in Salmon and Talley (1989) in order to ensure that the advective fluxes are exactly energy and enstrophy conserving in the absense of forcing and dissipation. The time stepping is carried out using a (nominally) fifth-order embedded Runge–Kutte Cash–Karp scheme (Press et al. 1992). In addition to providing better time accuracy compared to the usual leapfrog time discretization, this forward-time discretization obviates the need for time-filtering used to remove the computational mode in the leapfrog discretization.

3. Model results

The model experiments are summarized in Table 1. We consider two different Rossby numbers, free-slip and superslip boundary conditions, and the effect of using Laplacian or biharmonic mixing. All the experiments are eddy-resolving and are run for 100 nondimensional time units, a unit of time being the turnover time for a basin-scale gyre circulating at the Sverdrup velocity (see the nondimensionalization used in the previous section).

Figure 2 shows the instantaneous streamfunction and potential-vorticity fields at time 90 from run 1. Laplacian mixing of momentum with a Munk scale of 0.04 was used in conjunction with free-slip boundary conditions. The figure demonstrates the vigorous eddying nature of the flow. The strong distortion of the potential vorticity contours is indicative of an active potential enstrophy cascade in the domain interior, a point we shall return to later.

Figure 3 shows contour plots of the time-averaged streamfunction and potential vorticity fields for the same run. The averaging excluded the first 20 units of time. This ensures that the averaging is carried out over a period in which the flow field is statistically steady, as can be verified by reference to Fig. 4 where the time series of the (kinetic) energy and potential enstrophy, normalized by their respective maxima, can be found. The time-mean circulation in Fig. 3 shows a four-gyre structure. The two inner gyres circulate in the same direction as conventional wind-driven gyres, while the two outer gyres at the northern and southern ends of the basin circulate in the opposite direction.

To test the sensitivity to the choice of boundary condition, run 1 was repeated using the superslip boundary condition (7) (run 2). The instantaneous and time-averaged streamfunction and potential vorticity fields for run 2 are contoured in Fig. 5. (Whenever the instanta-

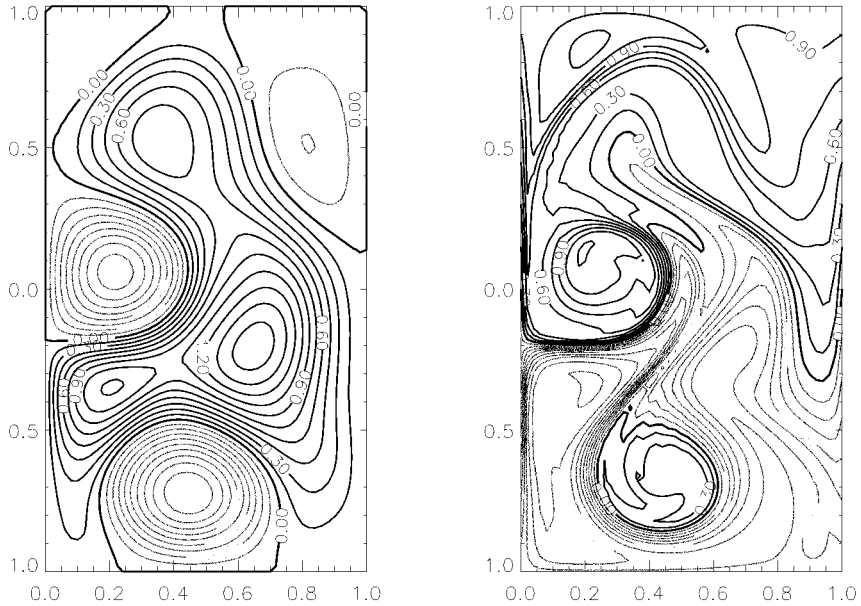

FIG. 2. Contour plots of the instantaneous nondimensional streamfunction (left panel) and potential vorticity (right panel) in eddy-resolving run 1. The contour interval for both streamfunction and potential vorticity is 0.15. Lighter lines are used for negative-valued contours and heavier lines for zero and positive-valued ones; this convention remains the same in all the contour plots to follow.

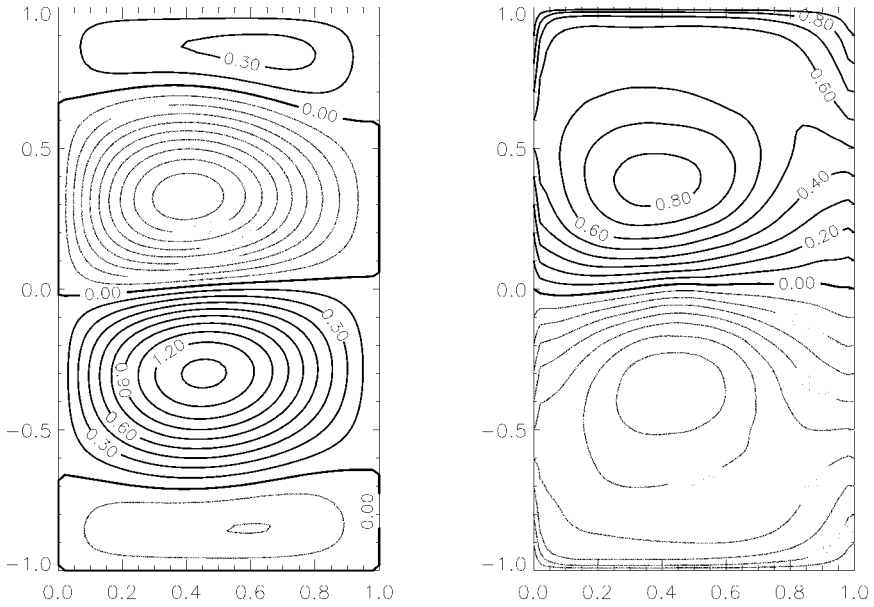

FIG. 3. The time-averaged, nondimensional streamfunction (left panel) and potential vorticity (right panel) in eddy-resolving run 1. The stream-function contour interval (SFCI) is 0.15, and the potential-vorticity contour interval (PVCI) is 0.10.

neous fields are shown, they are at time 90.) The remarkable similarity of the time-mean flow in this figure to that of run 1 (Fig. 3) indicates that the four gyre time-mean circulation is robust to the choice of either free-slip or superslip boundary conditions. As can be seen from Table 2 (discussed in detail later), the vorticity balance is dominated by the wind stress curl and the eddy flux of potential vorticity term, with the explicit dissipation playing a less important role. For the inner gyres, the eddy flux equilibriates the gyres, whereas for the outer gyres the eddy flux drives the gyres. The strong distortion of the mean potential vorticity field from lines of latitude indicates the strongly inertial character of the inner gyres. The tendency for potential vorticity to homogenise is evident, especially in the region occupied by the outer gyres.

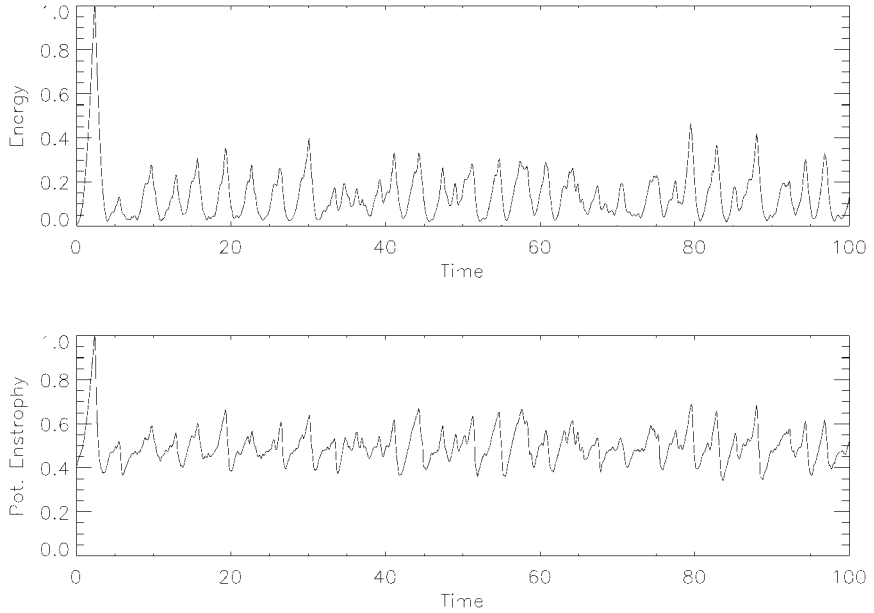

FIG. 4. Time series of energy (upper) and potential enstrophy (lower) normalized by their respective maxima. Statistical stationarity is established by time 10. Averaging to obtain the time-mean fields in Fig. 3 extends from time 20 to time 100.

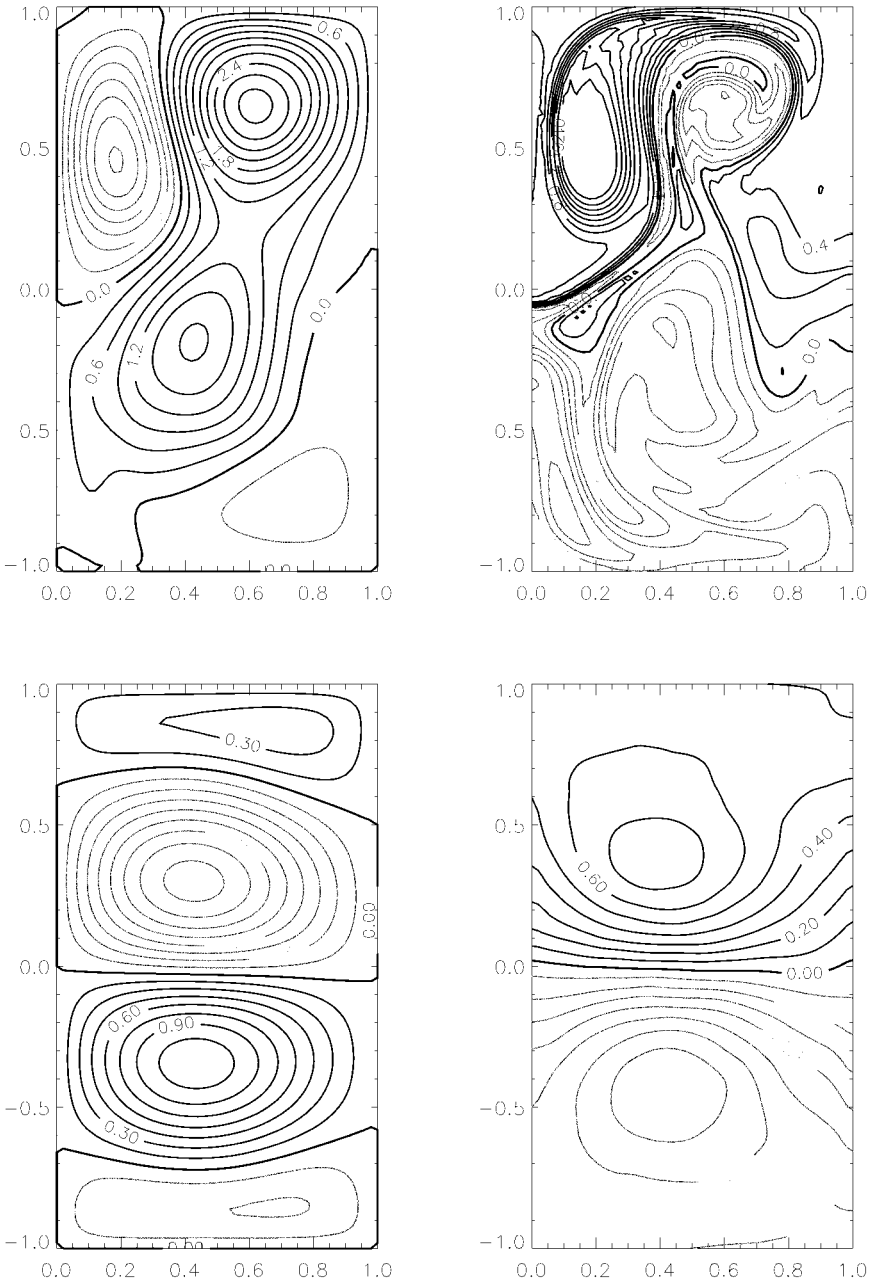

FIG. 5. Contour plots of the instantaneous (top panels) and time-averaged (bottom panels) streamfunction (left panels) and potential vorticity (right panels) for run 2. The only difference between the runs 1 and 2 is in the boundary conditions (free slip vs superslip). Instantaneous fields: SFCI is 0.30; PVCI is 0.20. Time-mean fields: SFCI is 0.15; PVCI is 0.10 (same as in Fig. 3).

TABLE 2. The mean vorticity balance for run 2 (in arbitrary units). The sum of the terms, which should be exactly zero, measures the error involved in computing the integrals from the model output (about 1% with respect to the dominant term).

Gyre	$\overline{J(\psi', q')}$	$\overline{F}$	$\overline{D}$	$-\overline{J(\psi', q')} + \overline{F} - \overline{D}$
Southern outer	−444.74	−434.22	14.18	−3.65
Subtropical wind-driven	−1092.50	−1141.88	−36.31	−13.06
Subpolar wind-driven	1157.18	1211.98	41.00	13.80
Northern outer	380.06	364.12	−18.87	2.93

Rhines and Holland (1979) have noted the importance of the cascade to small scales and subsequent dissipation of potential enstrophy for determining how potential vorticity is mixed by the eddies and the associated eddy/mean flow interaction. We noted earlier that there is an active potential enstrophy cascade in the domain interior, suggesting that the cascade and the dissipation of potential enstrophy, and hence the mixing of potential vorticity by the eddies, is not strongly influenced by the viscous boundary layers in our experiments but rather takes place primarily in the interior of the domain. Since the four-gyre structure is a consequence of the eddy flux of potential vorticity, it is likely that the four-gyre structure occurs even in cases when the Munk layer is not resolved by the model grid, as we have indeed demonstrated in other model runs. The robustness of the four-gyre structure is also supported by Fig. 7 in Scott and Straub (1998). This figure shows a four-gyre structure in the time-averaged field from an eddy-resolving experiment with very high resolution (the Munk layer is resolved by five grid points in their experiment). Scott and Straub (1998) therefore provide independent evidence of the four-gyre structure, although they make no comment on the presence of four gyres in their text. On the issue of model resolution, we note that Dukowicz and Greatbatch (1999) describe geostrophic turbulence experiments which use a special form of numerical side boundary condition chosen to ensure that both energy and potential enstrophy are dissipated on the numerical grid whatever the value of the viscosity. The numerical side boundary condition allows viscosity to be reduced to zero on a fixed grid without the need to resolve the Munk layer. In Dukowicz and Greatbatch (1999) the dissipation of potential enstrophy occurs in the interior of the domain and is entirely independent of the boundary layers.

Next, we address the issue of sensitivity to the form of the dissipation used. Run 3 uses biharmonic mixing of momentum with free-slip boundary conditions for the same Rossby number (0.01) and Munk scale (0.04) as in runs 1 and 2. Once again (Fig. 6) we see a four-gyre structure in the time mean fields and evidence of an active cascade in potential enstrophy in the domain interior.

So far, all cases have used a Rossby number 0.01. Next, we consider a Rossby number of 0.0016 (the associated Rhines scale is 0.04). We have done several runs with both Laplacian and biharmonic mixing at this Rossby number, all of which show the four gyre structure as before. As an example, we show run 4 in Table 1. This has biharmonic mixing with an associated Munk scale of 0.02 and uses the highest resolution (grid spacing 0.01 on a 101×201 grid) of any of our model runs. The model results show the same four gyre structure (Fig. 7) and also large regions of nearly uniform potential vorticity, especially in the region occupied by the outer gyres. The tendency for potential vorticity to homogenise was noted previously and can be seen in the other model experiments. Potential vorticity homogenization has also been noted in unforced geostrophic turbulence experiments (Cummins 1992; Wang and Vallis 1994; Dukowicz and Greatbatch 1999). Regions of uniform potential vorticity are associated with the emergence of the two separated gyres extending from the northern and southern boundaries of the model domain. These gyres correspond to the outer gyres found in our forced model experiments. An analysis of the gyres in terms of their meridional extent and the strength of the gyre circulation has been given by Cummins (1992) and Dukowicz and Greatbatch (1999).

Finally, in Fig. 8 the conventional double gyre structure is shown to occur at a higher value of Laplacian dissipation (run 6) for which the Munk and Rhines scales are comparable with each other. It should be noted that the flow in this case is turbulent (as can be seen in the plot of the instantaneous fields), although the eddies are not strong enough to drive outer gyres.

We now discuss the vorticity balance governing the four gyres. To do this, we first write $\psi = \overline{\psi} + \psi'$ and $q = \overline{q} + q'$, where overbar denotes time-averaged quantities and prime departures from the time average. In a statistically steady state, time averaging of (1) then gives

$$J(\overline{\psi}, \overline{q}) = -\overline{J(\psi', q')} + \overline{F} - \overline{D}. \qquad (11)$$

Integrating (11) over the area enclosed by a closed $\overline{\psi}$ streamline, the $J(\overline{\psi}, \overline{q})$ term drops out [this is the area integral version of the integral balance introduced by Niiler (1966) and which appears in Eq. (4.4) of Griffa and Salmon (1989)]. We are then left with a balance between the wind stress curl forcing $\overline{F}$, the dissipation $-\overline{D}$ and the divergence of the eddy flux of potential vorticity $-\overline{J(\psi', q')}$. These terms have been computed for each of the four gyres in Fig. 5 (run 2) using the $\overline{\psi} = 0$ contour to bound the region over which the integration is carried out. It is clear from the table, that the dominant balance is between the wind stress curl forcing and the eddy flux of potential vorticity term, with the explicit dissipation playing a negligible role. In the case of the two inner gyres, these circulate in the same sense as the wind stress curl and so can be considered as being driven by the wind forcing and equilibriated by the eddy flux of potential vorticity. The two outer gyres on the other hand circulate in the opposite sense to the wind stress forcing and are driven instead by the eddy forcing. Clearly, the stronger the eddy mixing compared with the wind forcing, the more homogeneous will be the potential vorticity within the individual gyres.

When comparing our results with those of Griffa and Salmon (1989) it is extremely important to realize that we are working in a regime in which the dissipation is sufficiently weak that the flow is highly turbulent and the eddy flux of potential vorticity dominates the vorticity balance over the explicit dissipation. Griffa and Salmon (1989) use Eq. (4.4) in their paper to argue that Fofonoff-type gyres will be inhibited in the barotropic vorticity equation under the conventional double-gyre

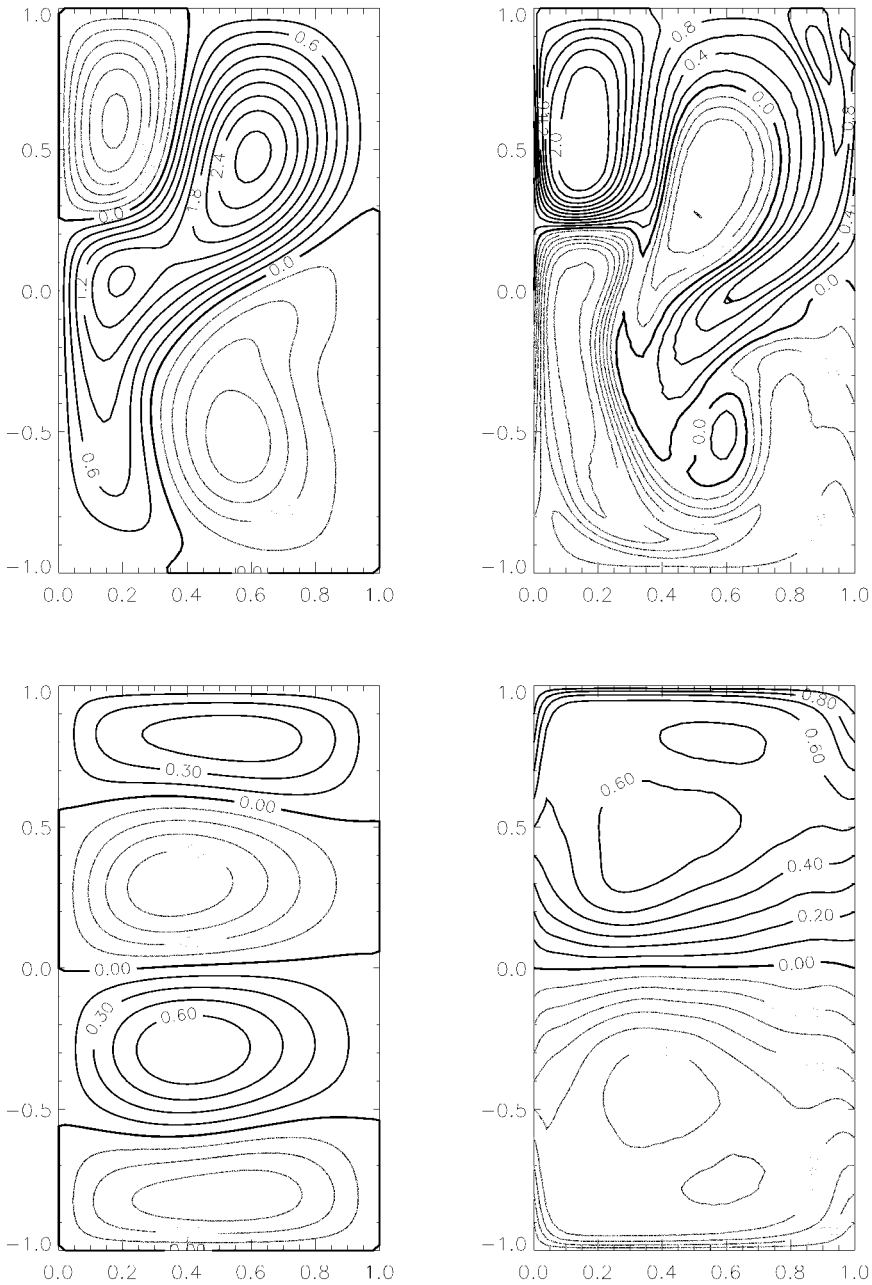

FIG. 6. Instantaneous (top panels) and time-averaged (bottom panels) streamfunction (left panels) and potential vorticity (right panels) fields for run 3. Rossby number is 0.01, as in the previous runs, but a biharmonic mixing of momentum with an associated Munk scale of 0.04 is used here. Instantaneous fields: SFCI is 0.30; PVCI is 0.20. Time-mean fields: SFCI is 0.15; PVCI is 0.10 (same as in Fig. 3).

wind forcing we use in our experiments. They note that Fofonoff-type gyres circulate in the opposite sense to the wind stress curl (as do the outer gyres in our model solutions) and so, for the case of a simple Rayleigh friction damping, the damping cannot balance the wind stress forcing in equilibrium. In our experiments, equilibrium is possible because the eddy flux of potential vorticity is large enough to close the balance. Since the explicit dissipation plays only a minor role in our experiments, the exact nature of the explicit dissipation is not important for our results. For example, it is not important that we have used lateral mixing, whereas Griffa and Salmon's argument uses Rayleigh friction as the damping. As it happens, we have also done some model runs (not shown), again in a highly turbulent regime, but using Rayleigh friction to provide the dis-

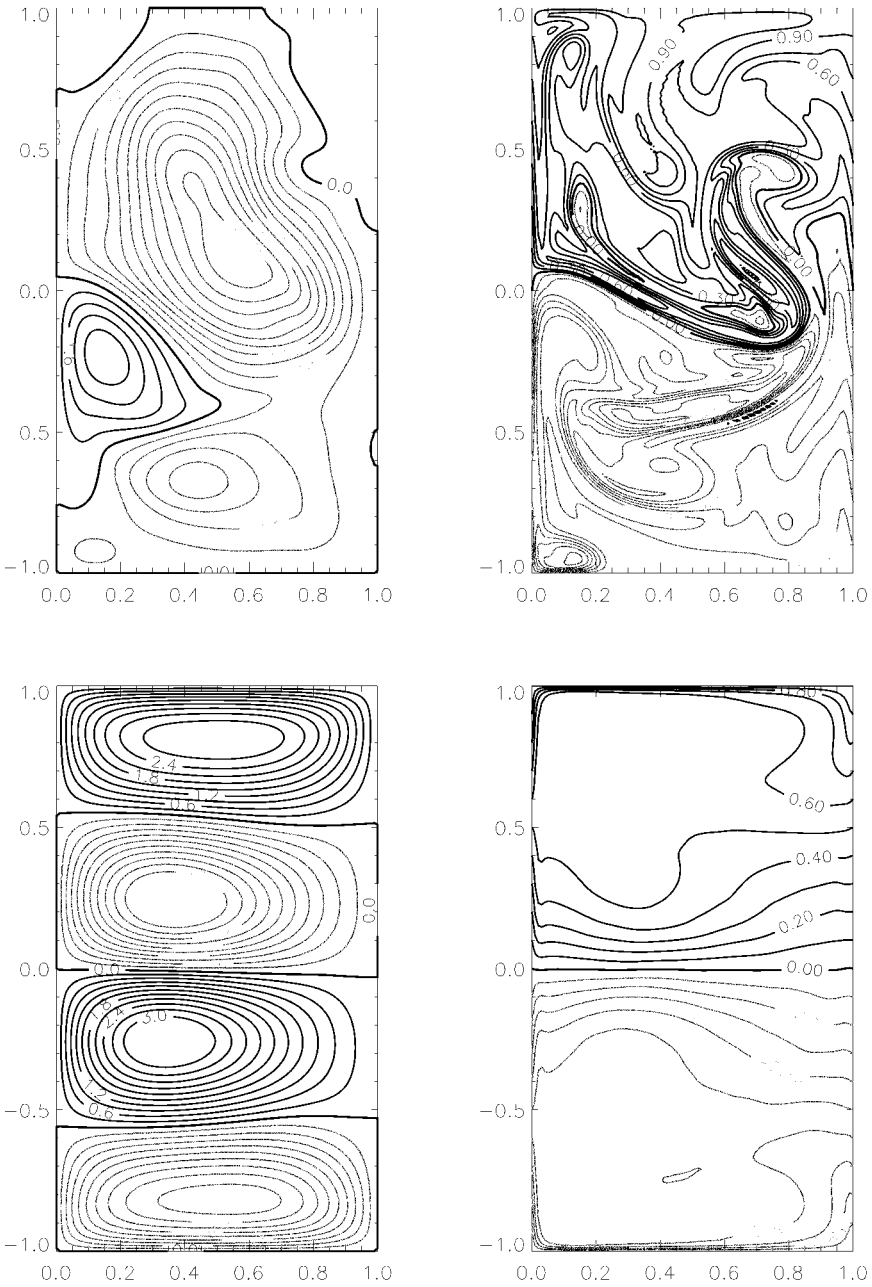

FIG. 7. Instantaneous (top panels) and time-averaged (bottom panels) streamfunction (left panels) and potential vorticity (right panels) fields for run 4. Instantaneous fields: SFCI is 0.80; PVCI is 0.15. Time-mean fields: SFCI is 0.30; PVCI is 0.10.

sipation. These experiments again show a four-gyre structure in the time mean fields. Once again, it is the eddy flux of potential vorticity that dominates the vorticity balance over the explicit dissipation.

4. The parameterized model

In our experiments, explicit dissipation plays a negligible role in the vorticity balance of the time-averaged state, encouraging us to try and mimic the time mean fields in the eddy resolving model using a parameterized model in which explicit dissipation is excluded, but including a simple parameterization of the eddy flux of potential vorticity. The vorticity balance inside any closed streamline is then, by design, between the wind stress curl forcing and the eddy flux of potential vorticity term, consistent with the dominant balance in Table 2. The model integrates (1) except that

$$D = \nabla \cdot (\kappa \nabla q) \tag{12}$$

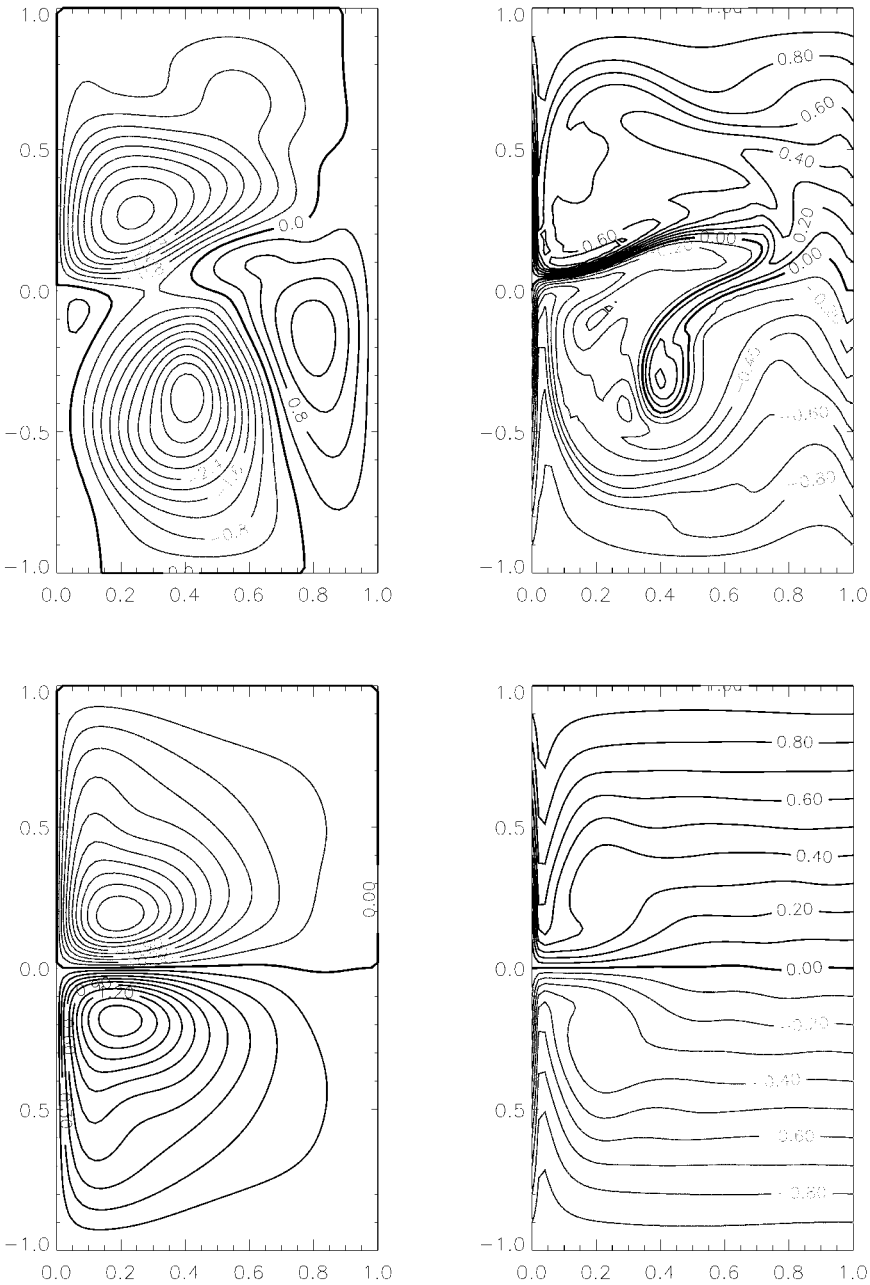

FIG. 8. Instantaneous (top panels) and time-averaged (bottom panels) streamfunction (left panels) and potential vorticity (right panels) fields for run 5. Since the Munk scale and inertial boundary layer scales are comparable, a conventional double-gyre results in the time-mean fields. Instantaneous fields: SFCI is 0.40; PVCI is 0.10. Time-mean fields: SFCI is 0.15; PVCI is 0.10 (same as in Fig. 3).

and along the boundary

$$\kappa \frac{\partial q}{\partial n} = 0. \tag{13}$$

The model variables are to be interpreted as time averages. Equation (12) parameterizes the divergent part of the eddy flux of potential vorticity as a down-gradient transfer, and the boundary condition (13) imposes a condition of no flux of potential vorticity through the boundary of the model domain (such a boundary condition is reasonable because the no normal flow boundary condition in the eddy-resolving experiments ensures that the normal component of $\overline{\mathbf{u}'q'}$ is zero along the boundary). To run the model with this form of boundary condition, it is necessary to update q on the boundary of the model domain, as with the superslip boundary

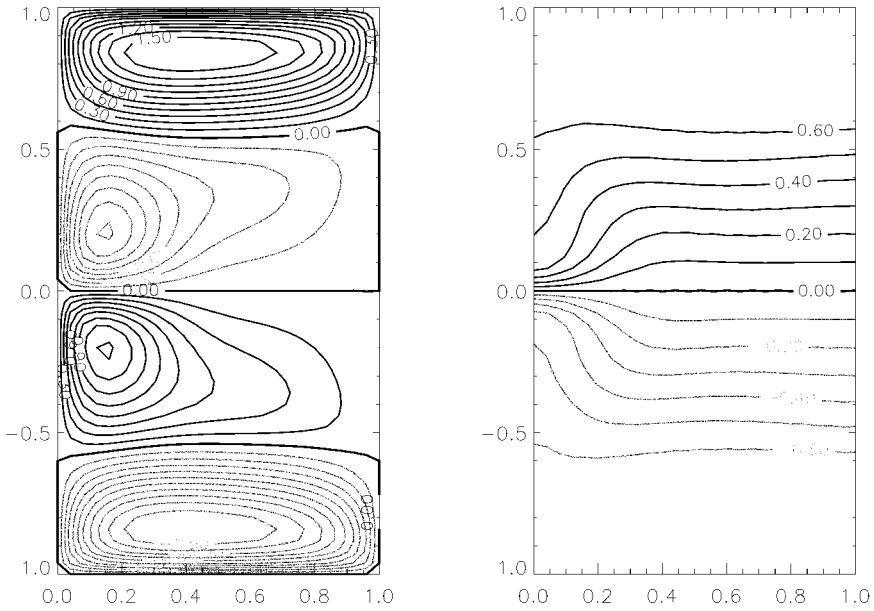

FIG. 9. The steady state fields from the parameterized model. Rossby number is 0.0016 and the dissipative term, a Laplacian mixing of potential vorticity (PV), arises from a parameterization of the divergence of the eddy pv-fluxes as a downgradient transfer of mean PV. The associated Munk scale is 0.08 and a no-normal-flux-of-PV boundary condition is used. The grid spacing is 0.04. SFCI is 0.15; PVCI is 0.10 (same as in Fig. 3).

condition used earlier. We also finite difference the q-mixing term (12) in such a way that when $F = 0$, the area integral of q over the model domain is conserved.

Figure 9 shows the steady state contours of streamfunction and potential vorticity obtained using the parameterized model. For simplicity, a spatially uniform κ is used with value corresponding to a Munk layer of width 0.08 (twice the grid spacing which is 0.04 in the parameterized model). The Rossby number for the experiment is 0.0016. The same four-gyre structure is found as in the time-mean circulation of the eddy-resolving experiments. In the parameterized model, the outer gyres are clearly associated with the regions of homogenised potential vorticity occupying the northern and southern quarters of the model domain. The correspondence between the presence of the outer gyres and the tendency for potential vorticity to homogenize was noted in the eddy-resolving experiments (e.g., compare Fig. 9 with the time-averaged fields in Fig. 7).

We can show that the four gyre structure is dependent on the boundary condition (13) by carrying out a model run identical to that used to produce Fig. 9 except that (13) is replaced by the superslip boundary condition in which the normal derivative of relative vorticity ζ, rather than the normal derivative of the potential vorticity $q = \zeta + \beta y$, is set to zero on the boundary. The resulting steady state shows only the conventional two-gyre structure. A similar result is obtained when a free-slip boundary condition is used. We have also carried out model runs in which κ is given by

$$\kappa = \kappa_0 \sin(\pi x/L) \cos(\pi y/2L). \qquad (14)$$

With this choice for κ, the boundary condition (13) is satisfied automatically without the need to apply a condition on the gradient of q or ζ. Again we see a four-gyre structure. These results emphasise the important role of the model boundaries in blocking the eddy flux of potential vorticity. The eddies can then erode the planetary vorticity gradient away from the northern and southern boundaries, leading to the emergence of the outer gyres.

5. Summary and discussion

We have seen that numerical experiments using a barotropic vorticity equation model in a highly turbulent regime, and driven by symmetric double gyre wind forcing, can produce a four-gyre structure in the time mean field, instead of the conventional two gyres. The outer gyres are driven by the eddy flux of potential vorticity and are found in experiments using either free-slip or superslip side boundary conditions, harmonic or biharmonic mixing of momentum and at two very different Rossby numbers. We have also found the four-gyre structure in eddy-resolving experiments that model the dissipation using a Rayleigh friction term (although we did not include results from these cases). An analysis of the vorticity budget for the four gyres shows that the explicit dissipation plays only a very minor role, the dominant balance being between the eddy flux of potential vorticity term and the wind stress curl. This encouraged us to carry out experiments using a parameterized model, which excludes the explicit dissipation,

but includes the divergent part of the eddy flux of potential vorticity as a downgradient transfer. A condition of no normal flux of potential vorticity is applied along the boundaries of the parameterized model. The parameterized model exhibits the same four-gyre structure. Experimentation with the parameterized model shows that in contrast to the eddy-resolving runs, the four-gyre structure is strongly dependent on the no normal flux condition applied to potential vorticity along the boundary. In particular, the four gyre structure is not found in the parameterized model when the superslip boundary condition of zero normal gradient in relative vorticity, or the conventional free slip boundary condition, is applied instead. This result emphasises that eddies mix potential vorticity and that it is the eddy flux of potential vorticity away from the northern and southern boundaries (through which the flux is zero) that is responsible for the emergence of the outer gyres.

One final comment, the outer gyres we are discussing here are very different from the inertial gyres associated with the inertial recirculation regions of ocean gyres (e.g., Niiler 1966; Marshall and Nurser 1986; Greatbatch 1987). The inertial recirculation gyres are associated with inertial gyres that circulate in the same sense as the wind forcing, not the opposite sense as do our outer gyres. Rather, the outer gyres in our experiments are more akin to the basin-scale, eddy-driven circulation envisaged by Holloway (1992), with the caviate that whereas Holloway's theory relies on statistical mechanics, the gyres we have found are associated with the tendency of eddies to erode the planetary vorticity gradient and homogenise potential vorticity (a detailed discussion of the connection with Holloway's theory can be found in Dukowicz and Greatbatch 1999).

Acknowledgments. Funding from the DOE CHAMMP Program is gratefully acknowledged. RJG would like to thank Los Alamos National Laboratory for hospitality and support during a two-month visit, and John Dukowicz for many stimulating discussions on this and related topics. Comments from reviewers led to considerable improvements in the manuscript.

REFERENCES

Arakawa, A., 1966: Computational design for long-term numerical integration of the equations of fluid motion: Two-dimensional incompressible flow: Part 1. *J. Comput. Phys.,* **1,** 119–143.

Bretherton, F. P., and D. B. Haidvogel, 1976: Two dimensional turbulence above topography. *J. Fluid Mech.,* **78,** 129–154.

Cessi, P., and G. R. Ierley, 1995: Symmetry-breaking multiple equilibria in quasigeostrophic wind-driven flows. *J. Phys. Oceanogr.,* **25,** 1196–1205.

Cummins, P. F., 1992: Inertial gyres in decaying and forced geostrophic turbulence. *J. Mar. Res.,* **50,** 545–566.

Dukowicz, J. K., and R. J. Greatbatch, 1999: Evolution of mean-flow Fofonoff gyres in barotropic quasigeostrophic turbulence. *J. Phys. Oceanogr.,* **29,** 1832–1852.

Greatbatch, R. J., 1987: A model for the inertial recirculation of a gyre. *J. Mar. Res.,* **45,** 601–634.

Griffa, A., and R. Salmon, 1989: Wind-driven ocean circulation and equilibrium statistical mechanics. *J. Mar. Res.,* **47,** 457–492.

Holland, W. R., T. Keffer, and P. B. Rhines, 1984: Dynamics of the ocean general circulation: the potential vorticity field. *Nature,* **308,** 698–705.

Holloway, G., 1992: Representing topographic stress for large-scale ocean models. *J. Phys. Oceanogr.,* **22,** 1033–1046.

Jayne, S. R., N. G. Hogg, and P. Malanotte-Rizzoli, 1996: Recirculation gyres forced by a beta-plane jet. *J. Phys. Oceanogr.,* **26,** 492–504.

Jiang, S., F.-F. Jin, and M. Ghil, 1995: Multiple-equilibria, periodic and aperiodic solutions in a wind-driven, double-gyre shallow-water model. *J. Phys. Oceanogr.,* **25,** 764–786.

Marshall, J. C., and A. J. G. Nurser, 1986: Steady, free circulation in a stratified, quasigeostrophic ocean. *J. Phys. Oceanogr.,* **16,** 1799–1813.

McCalpin, J. D., 1995: The statistics and sensitivity of a double-gyre model: The reduced-gravity, quasigeostrophic case. *J. Phys. Oceanogr.,* **25,** 806–824.

——, and D. B. Haidvogel, 1996: Phenomenology of the low-frequency variability in a reduced-gravity, quasigeostrophic double-gyre model. *J. Phys. Oceanogr.,* **26,** 739–752.

Nadiga, B. T., and D. D. Holm, 1997: Low-frequency variability in the double-gyre circulation. *Abstracts, Fourth SIAM Conf. on Applications of Dynamical Systems,* Snowbird, UT, SIAM, 20.

Niiler, P., 1966: On the theory of wind driven ocean circulation. *Deep-Sea Res.,* **13,** 597–606.

Ozgokmen, T. M., and E. P. Chassignet, 1998: Emergence of inertial gyres in a two layer quasigeostrophic ocean model. *J. Phys. Oceanogr.,* **28,** 461–484.

Press, W. H., B. P. Flannery, S. A. Teukolsky, and W. T. Vetterling, 1992: *Numerical Recipes in Fortran 77.* Cambridge University Press, 963 pp.

Rhines, P. B., and W. R. Holland, 1979: A theoretical discussion of eddy-driven mean flows. *Dyn. Atmos. Oceans,* **3,** 289–325.

——, and W. R. Young, 1982: Homogenization of potential vorticity in planetary gyres. *J. Fluid Mech.,* **122,** 347–367.

Salmon, R., and L. D. Talley, 1989: Generalization of Arakawa's Jacobian. *J. Comput. Phys.,* **83,** 247–259.

Scott, R. B., and D. N. Straub, 1998: Small viscosity behaviour of a homogeneous, quasi-geostrophic, ocean circulation model. *J. Mar. Res.,* **56,** 1225–1284.

Wang, J., and G. K. Vallis, 1994: Emergence of Fofonoff states in inviscid and viscous ocean circulation models. *J. Mar. Res.,* **52,** 83–127.